W-band TE_{01} gyrotron backward-wave oscillator with distributed loss

T. H. Chang,[1,a)] C. F. Yu,[1] C. L. Hung,[2] Y. S. Yeh,[3] M. C. Hsiao,[3] and Y. Y. Shin[3]
[1]*Department of Physics, National Tsing Hua University, Hsinchu, 300, Taiwan*
[2]*Department of Communication Engineering, National Penghu University, Penghu, Taiwan*
[3]*Department of Electro-Optical Engineering, Southern Taiwan University, Tainan, Taiwan*

(Received 9 April 2008; accepted 4 June 2008; published online 10 July 2008)

Distributed wall loss is proposed to enhance the stability and tunability of a *W*-band TE_{01} gyrotron backward-wave oscillator (gyro-BWO). Simulation results reveal that loss effectively suppresses the unwanted transverse modes as well as the high-order axial modes (HOAMs) without degrading the performance of a gyro-BWO that operates at the fundamental axial mode. Linear and nonlinear codes are used to calculate the interaction properties. The effects of the distributed loss on the starting currents of all of the modes of interest are discussed in depth. The interacting structure is optimized for stability. The calculated peak output power is 102 kW, corresponding to an efficiency of 20%. The 3 dB tuning bandwidth is 1.8 GHz, centered at 94.0 GHz when using 5 A and 100 kV electron beam. © *2008 American Institute of Physics*. [DOI: 10.1063/1.2950305]

I. INTRODUCTION

The gyrotron backward-wave oscillator (gyro-BWO) is a frequency-tunable source, which can be operated at high frequency and high power.[1–7] It has advanced greatly in the past few years because an increasing number of applications require frequency tunability, such as, electron spin resonance (ESR), plasma diagnostics, and enhancement of the sensitivity of nuclear magnetic resonance using dynamic nuclear polarization (DNP NMR). The oscillation of gyro-BWO is formed by internal feedback consisting of a forwardly moving electron beam and a backwardly propagating wave. The underlying physics is more complicated than that of resonant feedback, as in gyromonotron.[3] Contraction of the field profile at the nonlinear stage[8] which increases the threshold current of nonstationary behavior[9] were uncovered, enabling a gyro-BWO to operate stably and efficiently at high beam current. On the other hand, the electron transient angle was introduced to define the axial modes at the linear stage[10] and later found that an axial mode with a favorable field profile has been identified commonly to be dominant.[11] Recently, high efficiency operation of 29.8% employing a fundamental waveguide mode TE_{11} was reported at the *Ka*-band;[12,13] and a broadband tuning of 17% was demonstrated using a helical corrugated waveguide at the *X*-band.[14,15] Gyro-BWO has been demonstrated to be highly efficient and broadband, although separately. The next goal is to increase the operating frequency into the low terahertz range, which is associated with a highly overmoded condition. Severe mode competition is the major obstacle.

Figure 1 plots the $f-k_z$ diagram of a uniform interaction structure of radius 1.93 mm. The operating mode is the TE_{01} waveguide mode with fundamental cyclotron harmonic ($s=1$). The circular TE_{01} mode has the lowest propagating loss of all cylindrical waveguide modes, but it was chosen mainly because the mode converter has been successfully developed and the mode-selective circuit is relatively easy to construct. Major competing modes, for example, TE_{21}, TE_{31}, TE_{02}, TE_{61}, and TE_{32}, are also plotted. The parabolas are waveguide modes and the oblique lines are the beam-wave resonant conditions. The frequency can be tuned by changing either the magnetic field B_0 or the beam voltage V_b. To simplify the notation, an interacting point is represented as $TE_{mn}^{(s)}$, where the subindices m and n are the mode indices and the superscript (s) is the cyclotron harmonic number. For example, the operating mode is denoted $TE_{01}^{(1)}$. At the low magnetic field, $TE_{21}^{(1)}$ might be the greatest threat to the operating mode; while at the high magnetic field, $TE_{31}^{(1)}$ is the major competitor. Other second harmonic competing modes include $TE_{02}^{(2)}$, $TE_{61}^{(2)}$, and $TE_{32}^{(2)}$. Luckily, the interaction strengths of the second harmonic are weaker compared to those of the fundamental harmonic.

In addition to transverse mode competition, however, axial mode competition occurs. The operating mode $TE_{01}^{(1)}$ can be further classified into different axial modes ($\ell=1,2,3\ldots$) based on the concept of the electron transit angle.[10] A mode with a favorable field profile, normally the fundamental axial mode, tends to be the dominant axial mode, which determines the axial mode competition.[11] Recently, the distributed loss was found to be effective in selectively suppressing the competing axial modes of TE_{11} at the transient state.[16] The distributed loss scheme was adopted to achieve a smooth and stable tuning and the effect of this approach on the suppression of the competing modes was discussed.

The distributed wall loss was demonstrated to be an effective means of suppressing spurious oscillations in gyro-TWTs.[17–19] The major spurious oscillations, caused by the absolute instabilities, are effectively stabilized by coating the distributed loss at the upstream end of the interaction waveguide. This study takes advantage of this fact, but the distributed loss is applied on the downstream wall to stabilize the competing transverse and axial modes. Finally, the nonlinear behavior, the magnetic field, and beam voltage tunings at 5 A, are shown.

[a)]Electronic mail: thschang@phys.nthu.edu.tw.

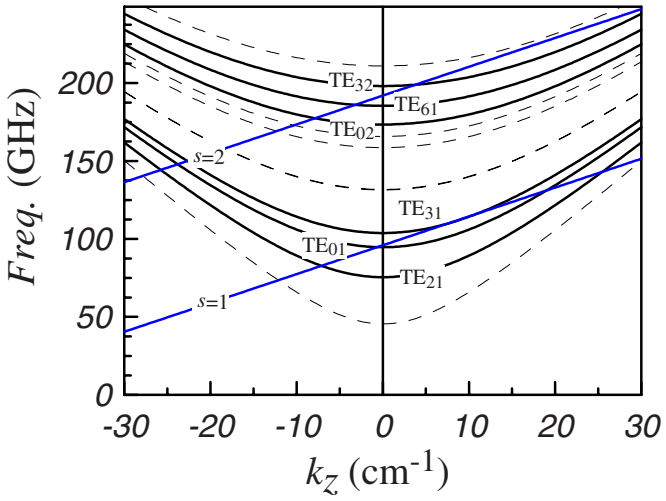

FIG. 1. (Color online) Frequency vs k_z diagram of the fundamental harmonic TE_{01} gyro-BWO with a waveguide radius r_w of 0.193 cm. The parabolas represent the transverse waveguide modes TE_{mn} and the oblique lines denote the beam-wave resonance lines.

II. GEOMETRY AND FIELD PROFILES

A. Numerical model

Figure 2 shows the beam-wave coupling strength for the six transverse modes of interest. Generally speaking, the fundamental cyclotron harmonic ($s=1$, solid lines) normally exhibits stronger coupling than the second cyclotron harmonic ($s=2$, dashed lines). Properly choosing the guiding center position of the electron beam (r_c) can alleviate the mode competition. In a uniform interaction structure, the optimal guiding center position of $TE_{01}^{(1)}$ is 0.48 r_w, where r_w is the waveguide radius. Tapering the interacting structure might enhance the interaction efficiency as well as slightly broaden the tuning range. In this study, a tapered structure is used. Hence, the guiding center radius of the beam ranges from 0.463 to 0.473 r_w. For such a guiding center radius, the major competing transverse modes are $TE_{21}^{(1)}$ and $TE_{31}^{(1)}$ as expected. The second cyclotron harmonic interactions are relatively

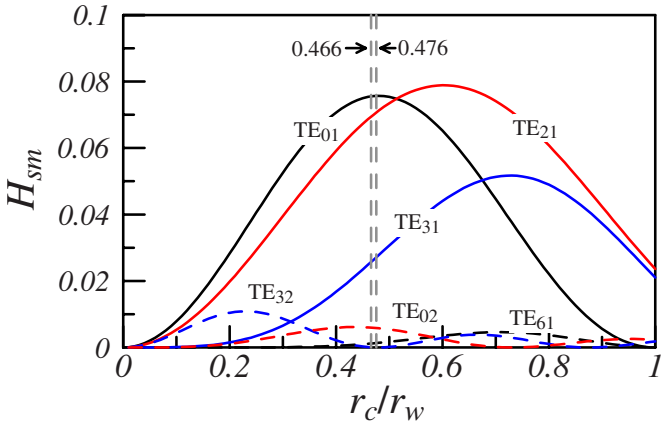

FIG. 2. (Color online) Beam-wave coupling strength vs guiding center position for the six transverse modes of interest. The modes that interact with fundamental cyclotron harmonic ($s=1$) and second cyclotron harmonic ($s=2$) are plotted as solid and dashed lines, respectively.

TABLE I. Simulation parameters.

Operating mode	$TE_{01}^{(1)}$ $\ell=1$
Competing transverse modes	$TE_{21}^{(1)}$, $TE_{31}^{(1)}$, $TE_{02}^{(2)}$, $TE_{61}^{(2)}$, $TE_{32}^{(2)}$
Competing axial modes	$TE_{01}^{(1)}$ $\ell=2,3,\ldots$
Tapered section length (L_1)	0.7–2.7 cm
Lossy section length (L_2)	0.2–0.6 cm
Waveguide radius (r_w)	0.189–0.193 cm
Beam current (I_b)	0–5 A
Beam voltage (V_b)	40–120 kV
Magnetic field (B_0)	38–44 kG
Guiding center position (r_c)	0.466–0.476 r_w
Velocity ratio ($\alpha=v_\perp/v_z$)	1
Velocity spread ($\Delta v_z/v_z$)	0%

weak, especially in the $TE_{32}^{(2)}$ mode. Accordingly, $TE_{01}^{(1)}$, $TE_{21}^{(1)}$, $TE_{31}^{(1)}$, $TE_{02}^{(2)}$, and $TE_{61}^{(2)}$ modes are considered hereafter.

A linear code[4] is adopted in conjunction with a nonlinear code.[8,20] The linear code is used to calculate the start-oscillation behavior. The calculated results are validated with the nonlinear code that is based on single-mode particle tracking in a weakly nonuniform interaction structure. The nonlinear code can also be used to find out the start-oscillation condition, but it is time-consuming. The linear code is especially useful in the early phase of the design. The electron beam interacts with the presumed waveguide mode (TE_{mn}). The beam parameters are determined by magnetron injection gun (MIG) simulation with a perpendicular-to-parallel velocity ratio $\alpha=1.0$ and a guiding center radius $r_c=0.09$ cm. The axial velocity spread ($\Delta v_z/v_z$) is assumed to be 0%. The cold beam assumption (0% spread) is generally valid when the operating frequency is close to the waveguide cutoff. Table I presents the simulation parameters.

B. Field profiles

Figure 3 shows the geometry and the linear field profiles of the gyro-BWO under study. Figure 3(a) depicts the interaction structure and the loss profile. The radius of the waveguide is slightly down tapered from 0.193 cm to 0.189 cm (taper angle 0.11°). In addition to the uniform section at both ends, it consists of two sections, a taper section (L_1, copper) and a lossy section (L_2, loss).

Figure 3(b) displays the normalized field profiles for the first three axial modes ($TE_{01}^{(1)}$, $\ell=1,2,3\ldots$). The field profiles with light loss (solid lines, $\rho=1\rho_{cu}$) and with heavy loss (dashed lines, $\rho=2\times10^4\rho_{cu}$) are calculated to study the effect of the distributed loss. The field profiles for the fundamental axial mode ($\ell=1$) differ slightly, because the bulk field and the loss profile are staggered. On the contrary, heavy loss significantly changes the field profiles of the HOAMs ($\ell=2$ and 3). A greater field bulk in the loss region corresponds to greater effectiveness of the mode suppression.

Figure 3(c) shows the field profiles for the major competing transverse modes, $TE_{21}^{(1)}$, $TE_{31}^{(1)}$, $TE_{02}^{(2)}$, and $TE_{61}^{(2)}$. Like $TE_{01}^{(1)}$, each transverse mode has several axial modes, but in most cases the fundamental axial mode ($\ell=1$) has the lowest

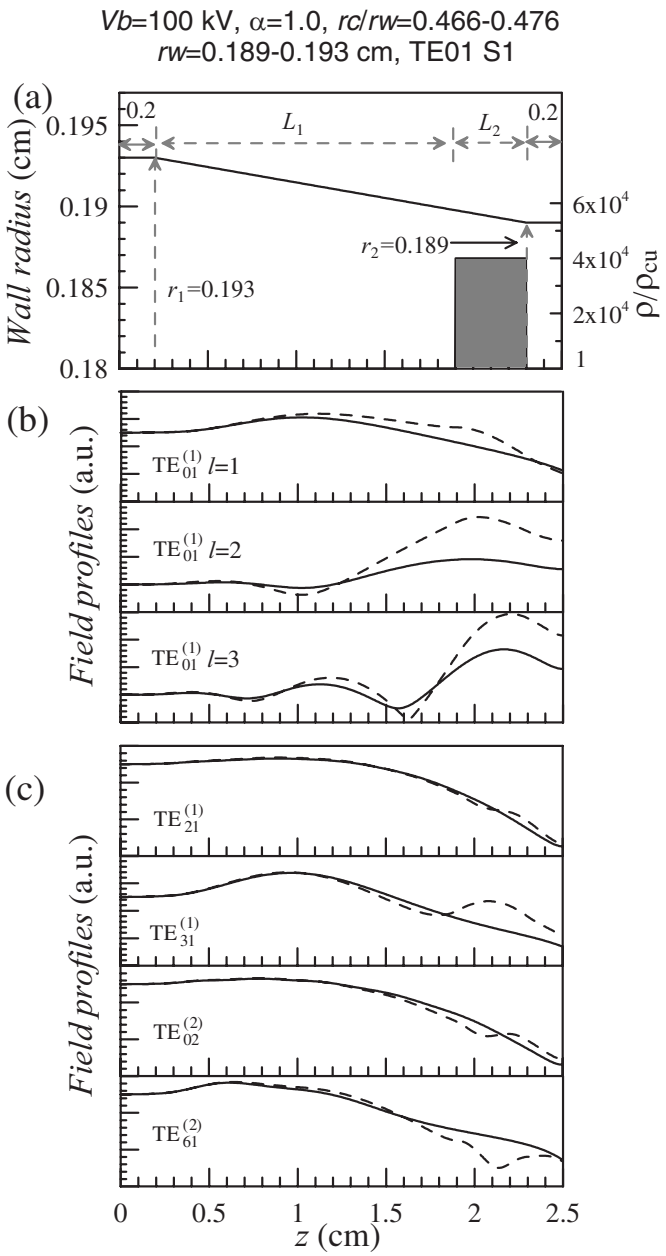

FIG. 3. (a) Interacting structure and profile of distributed loss. (b) Linear field profiles of first three axial modes ($\ell=1,2,3\ldots$) of $TE_{01}^{(1)}$. (c) Linear field profile of major competing transverse modes. The field profiles in parts (b) and (c) are normalized to the value at the beam entrance. The dashed curves and the solid curves represent cases with and without heavy losses, respectively. $V_b=100$ kV, $B_0=40.4$ kG; other simulation parameters are as listed in Table I. The following figures use the same simulation parameters, unless stated otherwise.

starting current. Therefore, only the fundamental axial mode is shown. The field profiles change slightly as expected when heavy loss is applied. Accordingly, the loss scheme is useful but not very effective to them. Compared to the operating mode $TE_{01}^{(1)}$ the competing modes consume more energy on the wall. Hence, the loss has a greater effect on the competing modes than on the operating mode in raising the oscillation thresholds.

Three parameters are to be determined: they are the distributed loss ρ, the taper section length L_1, and the lossy section length L_2. The effect of the distributed loss on the starting currents of the transverse modes and the axial modes are closely examined to determine these parameters.

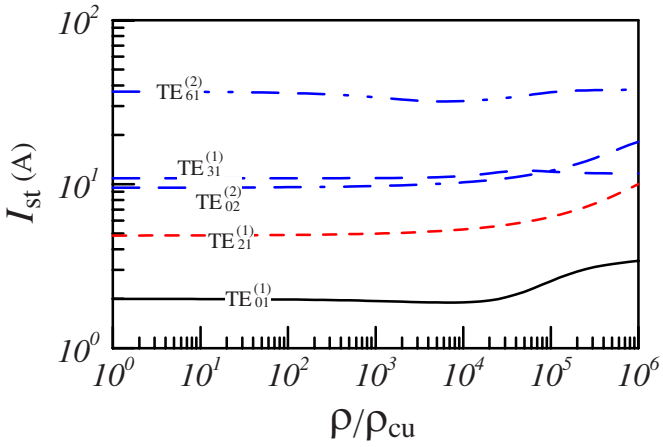

FIG. 4. (Color online) Starting currents of the modes of interest vs normalized loss. The distributed loss shortens the effective interacting length, and thus increases the starting currents.

III. EFFECT OF DISTRIBUTED LOSS

The gyro-BWO is relatively stable with a tapered interaction structure.[9,21] The nonlinear contraction of the field at the beam entrance allows it to be stably operated at a beam current that far exceeds the starting current. The single mode nonstationary behavior is not a serious problem provided the ratio of the operating current to the starting current is not too large. Therefore, this study concentrates on avoiding mode competition. The general criterion is that the starting currents of the competing modes must be greater than the operating current (such as, 5 A).

A. Transverse modes

Figure 4 shows the starting currents of the interested modes versus the normalized loss. The starting current of the desired mode $TE_{01}^{(1)}$ initially decreases slightly and then increases as the loss becomes heavier. Four competing modes, $TE_{21}^{(1)}$, $TE_{31}^{(1)}$, $TE_{02}^{(2)}$, and $TE_{61}^{(2)}$ exist, of which, the $TE_{21}^{(1)}$ mode has the lowest starting current. Thus, it is the most serious threat. Fortunately, the distributed loss increases the starting current of this mode. The greatest difference between the starting current of $TE_{01}^{(1)}$ and $TE_{21}^{(1)}$ mode is around 2×10^4 ρ_{cu}.

Figure 5 plots the starting currents versus the magnetic field for (a) light loss (1 ρ_{cu}) and (b) heavy loss (4×10^4 ρ_{cu}). The starting current is determined by two factors: the effective interaction length and the interaction strength. The behavior of $TE_{01}^{(1)}$ in Fig. 5(a) clearly indicates these two effects. As the magnetic field gradually raises, the effective length increases, reducing the starting current. As the magnetic field increases above a certain value (42.35 kG in this case), the interaction strength decreases, raising the oscillation threshold.

At the light loss case (1 ρ_{cu}), as shown in Fig. 5(a), the $TE_{21}^{(1)}$ mode sets the lower limits. Accordingly, the $TE_{01}^{(1)}$

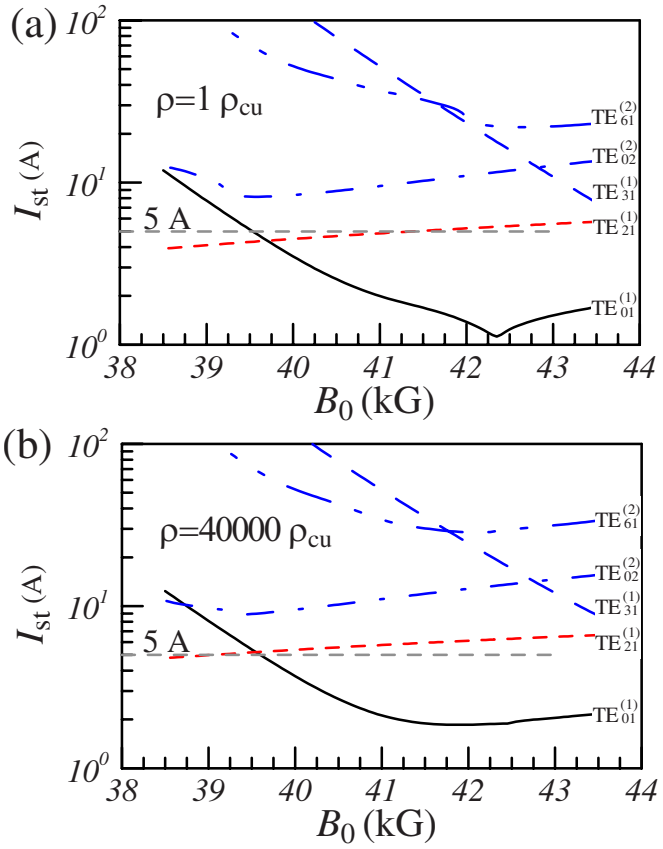

FIG. 5. (Color online) Start-oscillation current I_{st} of transverse modes vs magnetic field B_0 in two cases, (a) light loss $\rho=1\ \rho_{cu}$ and (b) heavy loss $\rho=4\times10^4\ \rho_{cu}$.

mode has to compete with the $TE_{21}^{(1)}$ mode at a current of 5 A (dashed line). With heavy loss, as in Fig. 5(b), such competition is removed. The starting current of the $TE_{21}^{(1)}$ mode is marginally higher than 5 A, revealing the effectiveness of the distributed loss. The $TE_{31}^{(1)}$ mode imposes an upper limit at high magnetic field region, but it is less critical because of the lower efficiency.

B. Axial modes

The dynamics of the beam-wave interaction determines the axial modes of the gyro-BWO. High-order axial modes (HOAMs, $\ell=2,3,\ldots$) tend to compete with the operating mode ($\ell=1$) when the beam currents exceed the start-oscillation currents of the former. The distributed loss has been demonstrated to be effective for the $TE_{11}^{(1)}$ mode operating at fundamental cyclotron harmonic.[16] The loss scheme is to be tested for the $TE_{01}^{(1)}$ mode.

Figure 6 plots the starting currents of the first three axial modes versus the normalized loss. As expected, the second axial mode ($\ell=2$) is the major competing mode. The bulk of the second axial mode is in the lossy region and so this mode is much more sensitive to the distributed loss than is the fundamental axial mode.

Figure 7 plots the starting current of the three axial modes as a function of the magnetic field for (a) light loss ($1\ \rho_{cu}$) and (b) heavy loss ($4\times10^4\ \rho_{cu}$). Light distributed loss [Fig. 7(a)] makes the second axial mode very problematic. It significantly limits the tunability at low magnetic field region. However, with heavy loss [Fig. 7(b)], such limitation has been removed. The distributed loss shortens the effective interaction length and thus significantly raises the starting currents of the HOAMs.

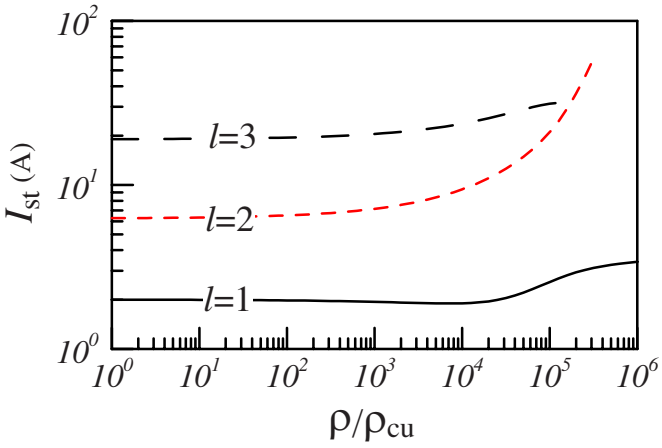

FIG. 6. (Color online) Start-oscillation currents I_{st} of the first three axial modes vs normalized loss. A higher axial mode index corresponds to greater starting current. The starting current of the major competing axial mode $\ell=2$ is significantly increased when the loss is applied.

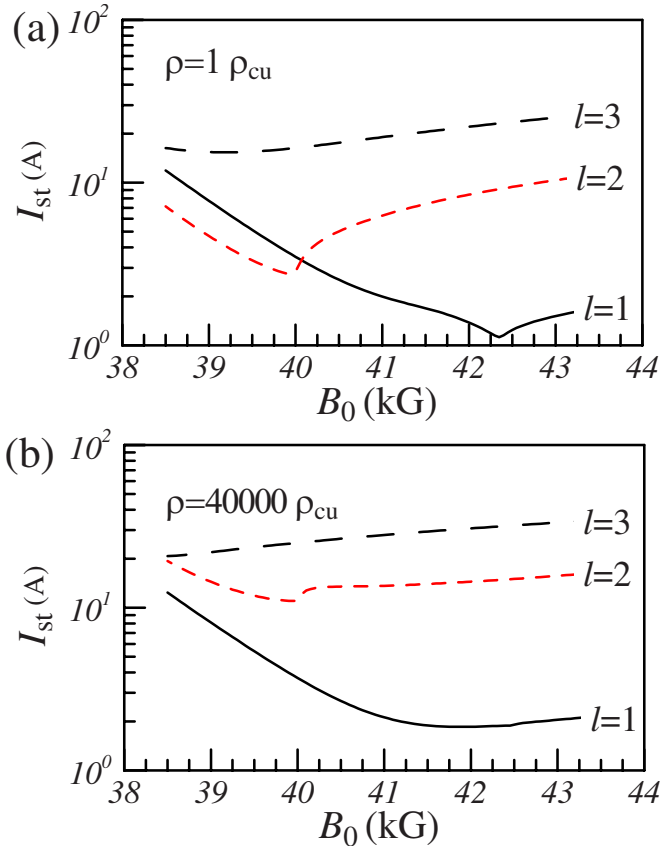

FIG. 7. (Color online) Start-oscillation currents I_{st} of first three axial modes vs magnetic field B_0 in two cases: (a) light loss $\rho=\rho_{cu}$ and (b) heavy loss $\rho=4\times10^4\ \rho_{cu}$. The loss smooths the curves of the starting currents by reducing the abruptness of the structural mismatch. The loss is very effective in raising the starting currents of HOAMs.

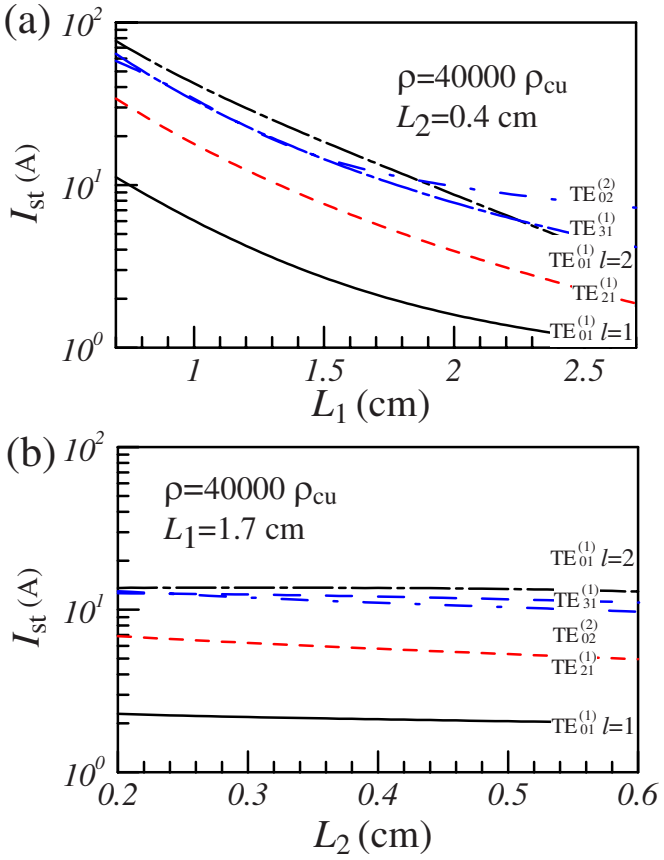

FIG. 8. (Color online) Starting currents I_{st} vs (a) taper section length L_1 and (b) lossy section length L_2. All of the modes of interest are plotted. The tapered structure causes the bulk interaction at the beam entrance, such that L_1 strongly affects the starting current. L_1 and L_2 are determined accordingly.

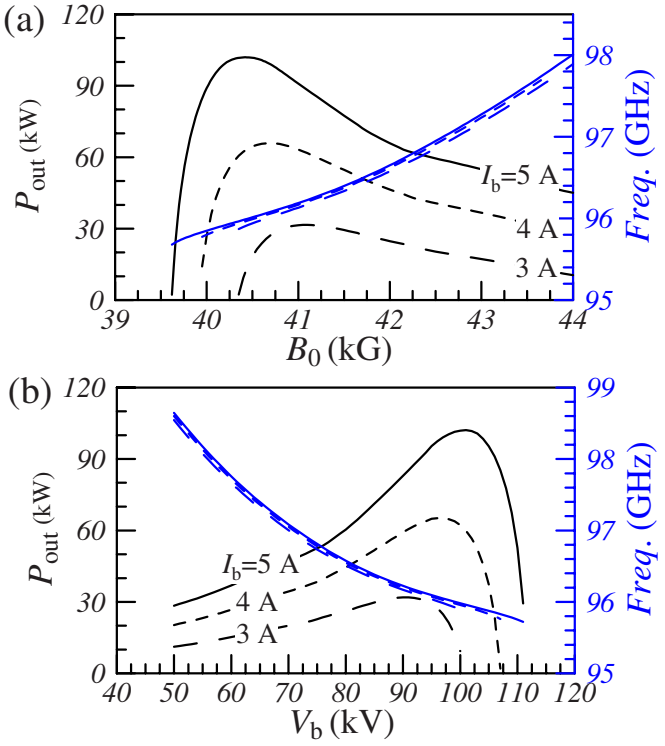

FIG. 9. (Color online) Calculated output power P_{out} and oscillation frequency f vs tuning parameters: (a) the magnetic field B_0 and (b) the beam voltage V_b. The interaction structure is shown in Fig. 3 and other parameters are listed in Table I.

Notably, the distributed loss is very effective to the HOAMs (Figs. 6 and 7), but not very useful to the competing transverse modes (Figs. 4 and 5). Applying a heavy loss slightly increases the starting currents of the transverse modes. The operating mode is marginally free from mode competition, implying that the distributed loss scheme is not a total solution. A mode-selective circuit is needed to suppress the competing transverse modes when a broader tuning range is required. Figures 4–7 reveal that a loss of 4×10^4 ρ_{cu} is a good choice for suppressing all of the competing modes. The next step is to determine the taper length (L_1) and the lossy length (L_2).

IV. OPTIMIZATION AND NONLINEAR BEHAVIOR

Figures 8(a) and 8(b) plot the starting current of the modes of interest against the taper length (L_1) and the lossy length (L_2), respectively. In Fig. 8(a), all of the starting currents are inversely proportional to L_1, as expected. A greater taper length L_1 corresponds to more serious mode competition. However, properly tapering the waveguide can enhance the efficiency of the gyro-BWO.[22–24] A taper section of 1.7 cm is a compromise between mode discrimination and efficiency. Figure 8(b) shows that the lossy section length (L_2) depends only weakly on the starting currents. A length of 0.4 cm is chosen.

In the present configuration, the competing axial and transverse modes are stabilized. Figure 9 plots output power and oscillation frequency as functions of (a) magnetic field B_0 and (b) beam voltage V_b. The calculated results show that the peak output power of the stable $TE_{01}^{(1)}$ gyro-BWO is 102 kW when using 5 A and 100 kV electron beam, corresponding to an efficiency of 20%. The oscillation frequency can be smoothly tuned. The 3 dB tuning range by the magnetic field is about 1.8 GHz. Figure 9(b) presents the voltage tunings for 3 A, 4 A, and 5 A at B_0=40.4 kG. Both magnetic and voltage tunings look acceptable.

V. CONCLUSIONS

The competing transverse and axial modes, which limit broadband tuning and high efficiency operation, are stabilized using the distributed loss scheme. Applying the distributed loss in the downstream of an interaction region raises the starting currents of the non-TE_{01} transverse modes by increasing the energy consumption on the lossy wall. It also shortens the feedback loop of the HOAMs ($TE_{01\ell}$, $\ell>1$). Properly employing the distributed loss suppresses the competing modes. It is not only useful to the gyrotron traveling-wave amplifier tube (gyro-TWT), but also effective to the gyro-BWO. The calculated results reveal that the *W*-band gyro-BWO is promising. The maximum output power is 102 kW with a 3 dB tuning bandwidth of 1.8 GHz. The experiment is ongoing. The high-performance TE_{01} mode converter is ready, but the magnetron injection gun (MIG) is still being designed.

ACKNOWLEDGMENTS

The authors would like to thank Professor K. R. Chu, Dr. K. F. Pao, and Dr. C. C. Chiu for many valuable comments. The National Center for High-Performance Computing (NCHC) is commended for providing computing facilities and technical supports. Mr. Ted Knoy is appreciated for his editorial assistance.

This work was sponsored by the National Science Council of Taiwan.

[1] G. S. Nusinovich and O. Dumbrajs, IEEE Trans. Plasma Sci. **24**, 620 (1996).
[2] J. M. Wachtel and E. J. Wachtel, Appl. Phys. Lett. **37**, 1059 (1980).
[3] K. R. Chu, Rev. Mod. Phys. **76**, 489 (2004).
[4] C. S. Kou, Phys. Plasmas **1**, 3093 (1994).
[5] S. Y. Park, R. H. Kyser, C. M. Armstrong, R. K. Parker, and V. L. Granatstein, IEEE Trans. Plasma Sci. **18**, 321 (1990).
[6] A. K. Ganguly and S. Ahn, Int. J. Electron. **67**, 261 (1989).
[7] A. T. Lin, Phys. Rev. A **46**, R4516 (1992).
[8] S. H. Chen, K. R. Chu, and T. H. Chang, Phys. Rev. Lett. **85**, 2633 (2000).
[9] T. H. Chang, S. H. Chen, L. R. Barnett, and K. R. Chu, Phys. Rev. Lett. **87**, 064802 (2001).
[10] S. H. Chen, T. H. Chang, K. F. Pao, C. T. Fan, and K. R. Chu, Phys. Rev. Lett. **89**, 268303 (2002).
[11] K. F. Pao, T. H. Chang, C. T. Fan, S. H. Chen, C. F. Yu, and K. R. Chu, Phys. Rev. Lett. **95**, 185101 (2005).
[12] T. H. Chang, C. T. Fan, K. F. Pao, and K. R. Chu, Appl. Phys. Lett. **90**, 191501 (2007).
[13] C. T. Fan, T. H. Chang, K. F. Pao, S. H. Chen, and K. R. Chu, Phys. Plasmas **14**, 093102 (2007).
[14] W. He, A. W. Cross, A. D. R. Phelps, K. Ronald, C. G. Whyte, S. V. Samsonov, V. L. Bratman, and G. G. Denisov, Appl. Phys. Lett. **89**, 091504 (2006).
[15] W. He, K. Ronald, A. R. Young, A. W. Cross, A. D. R. Phelps, C. G. Whyte, E. G. Rafferty, J. Thomson, C. W. Robertson, D. C. Speirs, S. V. Samsonov, V. L. Bratman, and G. G. Denisov, IEEE Trans. Electron Devices **52**, 839 (2005).
[16] K. F. Pao, C. T. Fan, T. H. Chang, C. C. Chiu, and K. R. Chu, Phys. Plasmas **14**, 093301 (2007).
[17] K. R. Chu, H. Y. Chen, C. L. Hung, T. H. Chang, L. R. Barnett, S. H. Chen, and T. T. Yang, Phys. Rev. Lett. **81**, 4760 (1998).
[18] H. H. Song, D. B. McDermott, Y. Hirata, L. R. Barnett, C. W. Domier, H. L. Hsu, T. H. Chang, W. C. Tsai, K. R. Chu, and N. C. Luhman, Jr., Phys. Plasmas **11**, 2935 (2004).
[19] Y. S. Yeh, Y. Y. Shin, Y. C. You, and L. K. Chen, Phys. Plasmas **12**, 043108 (2005).
[20] Y. S. Yeh, T. H. Chang, and T. S. Wu, Phys. Plasmas **11**, 4547 (2004).
[21] G. S. Nusinovich, A. N. Vlasov, and T. M. Antonsen, Jr., Phys. Rev. Lett. **87**, 218301 (2001).
[22] M. T. Walter, R. M. Gilgenbach, P. R. Menge, and T. A. Spencer, IEEE Trans. Plasma Sci. **22**, 578 (1994).
[23] C. S. Kou, C. H. Chen, and T. J. Wu, Phys. Rev. E **57**, 7162 (1998).
[24] M. T. Walter, R. M. Gilgenbach, J. W. Luginsland, J. M. Hochman, J. I. Rintamaki, R. L. Jaynes, Y. Y. Lau, and T. A. Spencer, IEEE Trans. Plasma Sci. **24**, 636 (1996).